

## Field Effect Transistors based in a $\text{Sn}_3\text{O}_4$ nanobelt

Rosana Alves Gonçalves<sup>\*1</sup>, Leonardo Martins do Amaral<sup>2</sup>, Maurício Ribeiro Baldan<sup>3</sup>, Adenilson José Chiquito<sup>2</sup>, Olívia Maria Berengue<sup>1</sup>

<sup>1</sup> LCCTnano - Department of Physics and Chemical, São Paulo State University (UNESP), School of Engineering, CEP 12.516-410, Guaratinguetá, São Paulo, Brazil. <sup>2</sup> NanOLaB - Department of Physics, Federal University of São Carlos (UFSCAR), CEP 13.565-905, São Carlos, São Paulo, Brazil. <sup>3</sup> LAS-CMS - Department of Space Engineering and Technology, National Institute of Space Research (INPE), CEP 12.227-010, São José dos Campos, São Paulo, Brazil.

<sup>\*</sup>rosana703@gmail.com

Keywords:  $\text{Sn}_3\text{O}_4$  nanobelt, semiconductor, field effect transistor

### Abstract

In this work, high quality single crystalline  $\text{Sn}_3\text{O}_4$  nanobelts grown by the vapor-solid (VS) method associated to a carbothermal reduction process were studied. Field Effect Gun Scanning Electronic Microscopy confirmed the growth of belt-like nanostructures by the VS method. X-Ray Diffraction revealed that the synthesis resulted in monocrystalline belts of high crystalline quality and preferential growth orientation. Semiconductor character of samples was detected by temperature-dependent resistivity measurements and the variable range hopping (VRH) was found to be the main mechanism of electronic transport in a large range of temperatures. A Field Effect Transistor (FET) based in a single nanobelt of  $\text{Sn}_3\text{O}_4$  was built in order to obtain key parameters of the nanobelt since it is the active channel in the device. The transistor was characterized by current-voltage curves from which we found the  $\text{Sn}_3\text{O}_4$  channel to be n-type. The density of free carriers was found to be  $5,07 \times 10^{17} \text{ cm}^{-3}$  and mobility was found to be  $11,5 \text{ cm}^2/\text{V.s}$ . The field effect properties of the  $\text{Sn}_3\text{O}_4$  nanobelts were also studied under UV illumination. The results indicate that the conductance is an order of magnitude greater in this condition than in dark and this photoconductive behavior was associated to the presence of oxygen vacancies in  $\text{Sn}_3\text{O}_4$  structure releasing free carriers to the channel.

### Introduction

In recent years, nanostructured transparent conductive oxides (TCOs) have been extensively studied because of its potential applications in electronic and optical devices [1-3]. Currently, special attention has been given to some non-stoichiometric phase of tin oxide specially  $\text{Sn}_3\text{O}_4$ , because it has band gap in the visible portion of the electromagnetic spectrum (2, 9 eV) [4].

The electrical behavior of  $\text{Sn}_3\text{O}_4$  nanobelts was recently found to be driven by oxygen vacancies defects leading to the observation of phonon scattering in a wide range of temperatures [5].

Also it was found that non-stoichiometric  $\text{Sn}_3\text{O}_4$  has shown interesting catalytic properties: this material was effective in the degradation of methyl orange (irradiated with visible light) [6] and presents an  $\text{H}_2$  evolution rate in aqueous solution comparable to the usual light sensitive photocatalysts [7].

The combination of these properties with the fact that it is a non-toxic [8] material it can said that  $\text{Sn}_3\text{O}_4$  is an excellent candidate to be applied in gas sensors [9,10], lithium ion batteries [11], and photocatalysts [12].

Besides, its great potential to be applied in electrical and photocatalytic it can be said that  $\text{Sn}_3\text{O}_4$  has not been fully explored.

Hoping to add data to fully understand the properties of this tin oxide nanostructured material in this work we explored structural and electronic characterization of non-stoichiometric  $\text{Sn}_3\text{O}_4$  nanobelts. By constructing a field effect transistor based in a single nanobelt we found an n-type behavior for the active channel and key parameters of this device such as mobility and on/off ratio were found.

As we know,  $\text{Sn}_3\text{O}_4$  nanobelts exhibit great responsivity to the ultraviolet light [5] and this photoconductive behavior was associated to the presence of oxygen vacancy in its structure. In this sense, we analyze the behavior of the field effect transistor under UV illumination. The results indicate an increase in channel conductance of about one order of magnitude caused by the releases of free carriers from oxygen vacancies.

### Methods and Results

The  $\text{Sn}_3\text{O}_4$  nanobelts were synthesized the vapor-solid mechanism in association with a carbothermal

reduction process. In this late process, the starting material is mixed with a carbon source in order to reduce the evaporation temperatures.

In this way we mixed  $\text{SnO}_2$  powder (Sigma Aldrich, > 325 mesh, purity > 99.9%) with graphite (Fluka, > 20  $\mu\text{m}$ , purity > 99%) 95:5 in weight, respectively. The final mixture was obtained after 72h mixing in a balls mill and was used as precursor material in the synthesis of the nanobelts.

The precursor powder was placed in an alumina crucible and inserted into the central region of an alumina tube positioned inside a horizontal tubular furnace (Lindberg/Blue M) where the temperature, gas flux and evaporation time were controlled. The furnace was heated to 1250°C (heating rate of 10°C/min) and it was maintained at this temperature for 2h before the cooling down to room temperature. A continuous flow of  $\text{N}_2$  (60 sccm) was maintained during the entire time of the synthesis.

Structural characterization of nanobelts was performed by X-Ray Diffraction by using a diffractometer (Rigaku, D-max 2500 model) with  $\text{Cu } K_\alpha$  radiation ( $\lambda = 1.54 \text{ \AA}$ ).

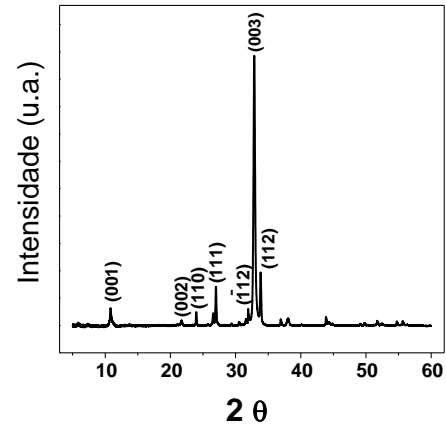
Initially, the device was fabricated to be performed for transport measurements. For this purpose the as-grow nanobelts were dispersed in ethanol, sonicated and deposited on an oxidized  $n^+$  Si wafer (500 nm). Then metal contacts were deposited on the top of the tips of nanobelts by using lithography techniques (Au/Ni, 100 nm, typical separation 5  $\mu\text{m}$ ). To reach the field effect transistor configuration a third metal contact was added to the back of this device (Al, 100 nm).

The transport measurements were carried out at different temperatures using a closed-cycle helium cryostat Janis, CCS 350 working at a pressure lower than  $5 \times 10^{-6}$  Torr. The resistance data was obtained using standard low-frequency ac lock-in AMETEK 7265 detection with great noise reduction.

The current-voltage data of the device were taken at 300K and were recorded by using two electrometers (Keithley 2400). The UV-dependent measurements were performed by using a 256 nm mercury lamp, 0.7  $\text{mW cm}^{-2}$ .

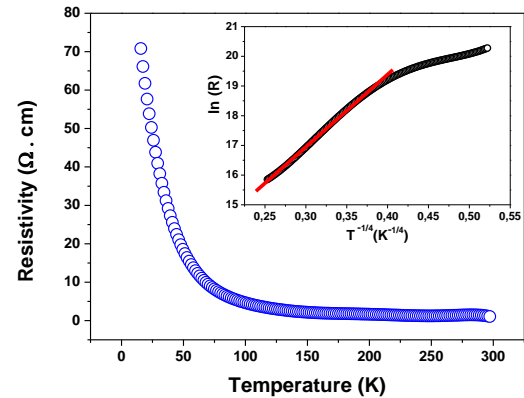
X-Ray Diffraction measurements of the as-grown samples are depicted in Figure 1.

**Figure 1.** X-Ray Diffraction of the as-grown  $\text{Sn}_3\text{O}_4$  nanobelts.



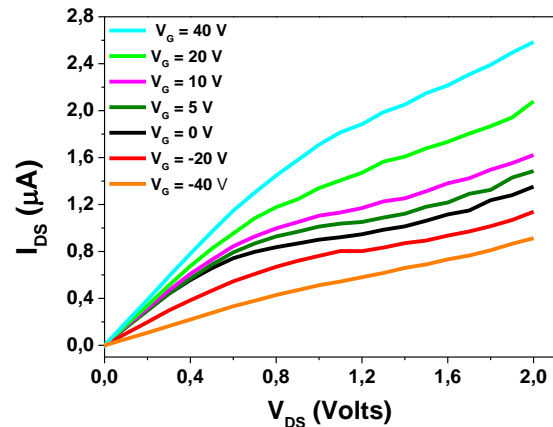
Temperature-dependent resistivity measurements are depicted in Figure 2.

**Figure 2.** Temperature-dependent resistivity measurements for the  $\text{Sn}_3\text{O}_4$  based device.



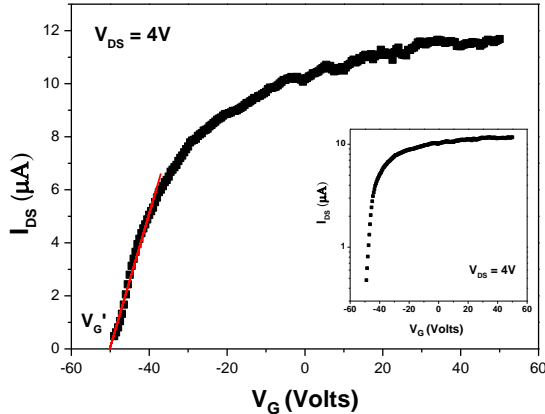
The transport measurements for the transistor were performed at room temperature. Figure 3 shows the  $I_{\text{DS}} \times V_{\text{DS}}$  curves for a single nanobelt with applied gate voltage ranging from -40 to 50 V.

**Figure 3.**  $I_{\text{DS}} \times V_{\text{DS}}$  measurements for a one- $\text{Sn}_3\text{O}_4$  nanobelt based device.



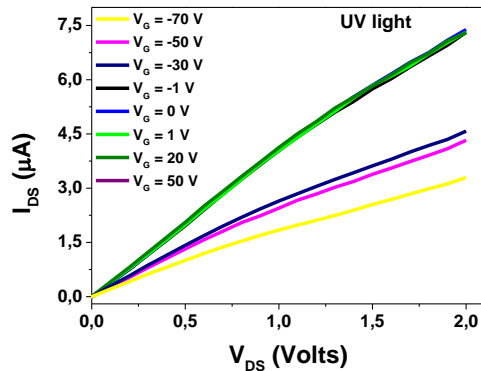
Measurements of  $I_{DS} \times V_G$  with fixed  $V_{DS}$  depicted in Figure 4 were made in order to obtain transistor key parameters such as: transconductance, mobility and on/off ratio.

**Figure 4.**  $I_{DS}$  versus  $V_G$  with  $V_{DS}$  fixed at 4 V showing the linear extrapolation used to calculate  $V_t$ . In the detail is showed semilog plot for to calculate subthreshold swing (S).



The FET performance was also studied under ultraviolet illumination as depicted in Figure 5.

**Figure 5.**  $I_{DS} \times V_{DS}$  curves showing the dependence of the FET response with UV light ( $\lambda = 256$  nm).



## Discussion

The  $\text{Sn}_3\text{O}_4$  nanobelts grown by VS transport method were submitted to X-Ray Diffraction technique in order to obtain data on the nanobelts' crystalline quality, the phase and structure. The XRD pattern (Figure 1) was indexed as the triclinic phase of  $\text{Sn}_3\text{O}_4$  (PDF#20-1293). The narrow and well defined peaks in the XRD indicate that the samples are single crystalline with high crystalline quality. The presence of a very intense peak related to planes (003) in the diffractogram is an indicative that

the sample presents a preferential growth orientation as reported in previous works [4] that identified the [001] direction by associating XRD data to Transmission Electron Microscopy data. The unrecorded peaks in the XRD correspond to small contributions of  $\text{SnO}$  and  $\text{SnO}_2$ . It is known that  $\text{Sn}_3\text{O}_4$  grows in a layered structure composed by  $\text{SnO}$  and  $\text{SnO}_2$  layers [13] and we believe that the observation of  $\text{SnO}$  and  $\text{SnO}_2$  peaks in our diffractogram are due to this growth mechanism.

The temperature-dependent resistivity features of the samples were explored and it was observed a semiconductor-like behavior: the resistivity decreases as the temperature increases.

Conduction in this material occurs by variable range hopping (VRH):

$$\rho(T) = \rho_0 \exp\left(\frac{T_0}{T}\right)^{1/4}, \quad (1)$$

where  $T_0 = 16\alpha^3/k_B N(E_F)$ , is a constant in which  $\alpha^{-1}$  is the localization length of wave function,  $k_B$  is the Boltzmann constant and  $N(E_F)$  is the density of states at the Fermi level [14]. The hopping model is based on the presence of a random potential that provides the location of electronic charge. Therefore, in the VRH process the charge transport requires a mechanism of conduction through localized states [15] in such way that electrons jump to neighboring sites of the comparable energy while phonons conserve energy. Since this process is assisted by phonons [4], a higher density of phonons in the structure implies an increase in hopping events.

The adjustment of this behavior (eq. 1) to the experimental data shows that this is the dominant transport mechanism for temperatures ranging from 40 to 297K (Figure 2).

The characterization of the nanobelt based transistor is shown in Figure 3. It can be seen from Figure 3 that conductance increases in the linear region from 3.3 for 4.6  $\mu\text{S}$  as the gate voltage varies from -40 to 40 V. This behavior in which the increase of gate bias causes the conductivity to grow is currently addressed to n-type channel transistors [16]. This is the first experimental measurement confirming the n-type semiconductor behavior of  $\text{Sn}_3\text{O}_4$  nanobelts reported previously by Suman et al [17].

In the FET configuration the current between the drain and the source is controlled by changing the voltage between the gate and drain contacts. In an n-type device a negative gate-source voltage increases the width of the depletion layer reducing the flow of carriers in the channel. When the depletion layer reaches its maximum, the gate voltage is no longer able to maintain a well-formed channel and the electrons tend to diffuse into the bulk before reaching the drain contact [18]. The current reaches the saturation regime and we say that the drain and source contacts are pinch-off [16].

In this regime, the current in the device is completely controlled by the gate voltage. In this case, the  $\text{Sn}_3\text{O}_4$  transistor did not reach the saturation regime or pinch-off, as observed in the  $I_{\text{DS}} \times V_{\text{DS}}$  curves. This is probably due to the excess of electrons in the channel originated from oxygen vacancy states: as the drain voltage increases the depletion layer is not large enough to limit the flow of electrons in the channel and the saturation regime is not achieved. This fact is a strong indication of a high density of carriers ( $n$ ) in the transistor channel.

Aiming to confirming this evidence and calculating key parameters for the transistor such as transconductance and mobility (of which  $n$  is dependent) measurements of  $I_{\text{DS}} \times V_{\text{G}}$  with fixed  $V_{\text{DS}}$  were performed. In the Figure 3 it is observed a plot of  $I_{\text{DS}} \times V_{\text{G}}$  for  $V_{\text{DS}} = 4 \text{ V}$  from it we calculated the threshold voltage ( $V_t$ ). The insert shows the even plot with vertical axis in logarithmic scale for to calculate the subthreshold swing ( $S$ ).

From of the curves depicted in Figure 4 the transconductance  $g_m = \frac{dI_{\text{DS}}}{dV_{\text{G}}}$  was calculated. Then, considering the value obtained for  $g_m$  and nanobelt's size and geometry the field effect mobility  $\mu_{\text{FET}}$  in the linear operation regime was calculated.

$$\mu_{\text{FET}} = \frac{g_m L^2}{C_{\text{OX}} V_{\text{DS}}} \quad , \quad (2)$$

with  $L = 7 \mu\text{m}$  and the capacitance of the back gate  $C_{\text{OX}}$  is  $5 \text{ fF}$  considering an approximation for cylindrical geometry. As a result we found the field effect mobility to be  $11,5 \text{ cm}^2/\text{V.s.}$

From resistivity measures presents and with the mobility data we calculate the carriers' density at  $300 \text{ K}$  by considering the following relationship:

$$\rho = \frac{1}{ne\mu} \quad (3)$$

From the eq. 3 we found  $n = 5,07 \times 10^{17} \text{ cm}^{-3}$ . The high value obtained confirms the assumption made to explain the absence of saturation regime in the transistor curves presented in Figure 1: the carrier's density is so high that the depletion layer cannot empty the channel.

The threshold voltage ( $V_t = V'_G + \frac{1}{2} V_{\text{DS}}$ ) [19] is an essential parameter for the transistor as it indicates the onset of significant drain current flow. In this case, as linear fit showed in Figure 4,  $V_t = -48 \text{ V}$  while the on/off ratio for this device was found to be  $10^2$ .

Important parameters such as device speed ( $v = L^2/\mu V$ ) [20] and subthreshold swing ( $S \equiv \Delta V_{\text{G}}/\text{decade } I_{\text{DS}}$ ) [16] were also calculated in order to fully characterize the  $\text{Sn}_3\text{O}_4$  based device. The obtained speed was found in the range of nanoseconds and  $S = 41 \text{ V/decade}$ . Lower values for

$S$  indicate higher speeds and lower power consumption for the FET.

The behavior of the field effect transistor was studied under UV illumination as showed in Figure 5. The  $I_{\text{DS}} \times V_{\text{DS}}$  curves depicts that current increases in the illuminated environment and cause an increase in channel conductance. The conductance (calculated from the linear region of the  $I_{\text{DS}} \times V_{\text{DS}}$  curves) increased from  $4.2$  to  $15.4 \mu\text{S}$  as the drain source bias varied from  $-2$  to  $2 \text{ V}$  with fixed  $V_{\text{G}} = 20 \text{ V}$  the device.

The oxygen vacancies present in the structure of the  $\text{Sn}_3\text{O}_4$  nanobelts are responsible for the observed photoconductive behavior. UV light excites electrons from oxygen vacancy states to the conduction band by increasing the current in the transistor channel. This characteristic of the device may be explored for the production of UV sensors.

All the characteristic parameters calculated for the field effect transistor based in single belt of  $\text{Sn}_3\text{O}_4$  are large enough for the use of the device in switching applications. Additionally, the photoconductive behavior of FET under UV illumination makes this device a promising candidate to be a light sensor.

## Acknowledgments

The authors would like to thank the Brazilian funding agencies FAPESP (FAPESP 2015/21816-4) and CNPq.

## References

- Wang, Z. L. *Annu. Rev. Phys. Chem.*, **2004**, *55*, 159.
- Lanfredi, A. J. C.; Galdes, R. R.; Berengue, O. M.; Leite, E. R. and Chiquito, A. J. *J. Appl. Phys.*, **2009**, *105*, 023708.
- Wan, Q.; Datoli, E. and Lu, W. *Small*, **2008**, *4*, 451-454.
- Berengue, O. M.; Simon, R. A.; Chiquito, A. J.; Dalmaschio, C. J.; Leite, E. R.; Guerreiro, H. A. and Guimarães, F. E. G. *J. Appl. Phys.*, **2010**, *107*, 033717.
- Berengue, O. M.; Kanashiro, M. K.; Chiquito, A. J.; Dalmaschio, C. J. and Leite, E. R. *Semicond. Sci. Technol.* **2012**, *27*, 065021.
- He, Y.; Li, D.; Chen, J.; Shao, Y.; Xian, J.; Zheng, X. and Wang, P. *RSC Advances*, **2014**, *4*, 1266-1269.
- Manikandan, M.; Tanabe, T.; Li, P.; Ueda, S.; Ramesh, G. V.; Kodiyath, R.; Wang, J.; Hara, T.; Dakshanamoorthy, A.; Ishihara, S.; Ariga, K.; Ye, J.; Umezawa, N. and Abe, H. *ACS Appl. Mater. Interfaces*, **2014**, *6*, 3790-3793.
- Song, H.; Son, S.Y.; Kim, S.K. and Jung, G. Y. I. *Nano Res.*, **2015**, *8*, 3553.
- Li, X.; Wang, F.; Tu, J.; Shah, H. U.; Hu, J.; Li, Y.; Lu, Y. and Xu, M. *J. Nanomater.*, **2015**, *2015*, 980170.
- Liua, J.; Wang, C.; Yanga, Q.; Gaoa, Y.; Zhoua, X.; Liang, X.; Sun, P. and Lu, G. *Sens. Actuators B*, **2016**, *224*, 128-133.
- Chen, X.; Huang, Y.; Zhang, K.; Feng, X. and Wei, C. J. *Alloys Compd.*, **2017**, *690*, 765-770.

- 12 Tanabe, T.; Hashimoto, M.; Mibu, K.; Tanikawa, T.; Gunji, T.; Kaneko, Abe, H.; Miyauchi, M. and Matsumoto, F. *J. Nanosci. Nanotechnol.*, **2017**, 17, 3454–3459.
- 13 Damaschio, C. J.; Berengue, O. M.; Stroppa, D. G.; Simon, R. A.; Ramirez, A. J.; Schreiner, W. H.; Chiquito, A. J. and Leite, E. R. *J. Crys. Growth*, **2010**, 312, 2881–2886.
- 14 N. F. Mott, *Metal-Insulator Transitions*, **1990**, (Taylor and Francis, London).
- 15 Hapert, J.J. V. Hopping conduction and chemical structure: a study on silicon suboxides, *PhD Thesis*, Utrecht University, **2002**.
- 16 Sze, S. M. *Physics of Semiconductor Devices*, **1981**, New York: Wiley.
- 17 Suman, P. H.; Felix, A. A.; Tuller, H. L.; Varela, J. A. and Orlandi, M. O., *Sens. Actuators B*, **2015**, 208, 122–127.
- 18 Jacoboni, C. *Theory of Electron Transport in Semiconductors: a Pathway from Elementary Physics to Nonequilibrium Green Functions*, **2010**, New York: Springer.
- 19 Ortiz-Conde, A.; Sánchez, F. J. G.; Liou, J. J.; Cerdeira, A.; Estrada, M. and Yue, Y. *Microelectronics Reliability*, **2002**, 42, 583–596.
- 20 Prins, M. W. J.; Grosse-Holz, K.-O.; Muller, G.; Cillessen, J. F. M.; Giesbers, J. B.; Weening, R. P. and Wolf, R. M. *Appl. Phys. Lett.*, **1996**, 68, 3650–3652.